Improvement in Stiffness Performance of Force Feedback Devices with Ultrasonic Motors*

Jian Song, *Student Member, IEEE*, Yuru Zhang, *Senior Member, IEEE* , Hongdong Zhang, Dangxiao Wang, *Senior Member, IEEE*, and Weiliang Xu, *Senior Member, IEEE*

***Abstract*—In the design of a haptic device, it is difficult to achieve simultaneously high stiffness and low friction and inertia. In our previous research, we proposed a co-actuation method to overcome this difficulty. The method uses a physical constraint to simulate hard contact and allows the device move freely in free motion space by keeping a clearance between the physical constraint and the link of the device. A stiffness of 40N/mm and back-driving friction of less than 0.3N have been achieved in a co-actuation module of one degree-of-freedom (DOF) using an electromagnetic motor and gear reducer. However, the stiffness is not high sufficient (10N/mm) at the initial contact due to the backlash in the transmission. In this paper, we explore the possibility to use an ultrasonic motor (USM) for solving this problem. Compared with the electromagnetic motor used in the early design, the USM is able to generate a larger resistant torque without gearbox, at a fast rate. We develop a model to determine the maximum clearance between the physical constraint and the link. We verify the clearance model and the force feedback performance using a one DOF haptic device. The experimental results show that the device achieves a stiffness of 61.5N/mm and back-driving friction less than 0.4N, which implies that the USM is promising for achieving both high stiffness and low friction and inertia required by the haptic application.**

I. Introduction

Haptic devices for force feedback mainly fall into two classes: impedance type and admittance type. The former is low in friction and inertia, thus being back-drivable. But they are usually limited in simulating large force and stiffness [1], [2]. The latter can simulate large force and stiffness, but not high in friction and inertia, thus being not back-drivable [3], [4]. The back driving force of a haptic device relies on both friction and inertia. In low speed, it is mainly affected by friction. While in high speed, inertia cannot be ignored. It is challenging to design a haptic device with both high stiffness and low friction and inertia, which is desirable in some applications. For example, in the virtual environment for dental surgery simulation, contacts between hard teeth and a light dental tool is a typical task to simulate. Thus, the haptic device needs to provide a hard contact (15.3-41.5N/mm [5]) with a low inertia [6].

*Research supported by the National Natural Science Foundation of China under the grant No. 61572055, and 61532003, and by National Key Research and Development Program of China under Grant No. 2017YFB1002803.

J. Song, Y. Zhang, H. Zhang and D. Wang are with State Key Lab of Virtual Reality Technology and Systems, Beihang University, No.37 Xueyuan Road, Haidian District, Beijing 100191, China (e-mail: yuru@buaa.edu.cn; hapticwang@buaa.edu.cn).

W. Xu is with the Department of Mechanical Engineering, The University of Auckland, Auckland 1010, New Zealand (e-mail: p.xu@auckland.ac.nz).

One solution to achieve high stiffness is using admittance type devices. For instance, Haptic Master has a stable stiffness range of 10-50 N/mm and a minimal tip inertia 2 kg [3]. By using a force sensor and appropriate control, the device can achieve a low back driving force without reducing the friction and inertia in actuation. As an alternative, we proposed a co-actuation method to achieve both high stiffness and low friction and inertia in [7]. We verified the method via a co-actuation module using an electromagnetic motor with a gear reducer. We found that the backlash in the gear reducer significantly decreases the stiffness of the module in the event of contact. In this paper, we explore the possibility to eliminate the effect of the backlash on the stiffness by using an ultrasonic motor (USM). Compared to electromagnetic motors, USMs are of low speed, high torque, quick response, and self-locking when powered off [8]. These advantages can make the USM directly drive the load without the gearbox, therefore eliminating the backlash in the transmission.

The USM has been used in haptic devices. To remove the stick and slip phenomenon at low speed, Giraud *et al.*[9], [10] developed a control algorithm for one DOF haptic knob using USM. A control of the traveling wave amplitude is achieved with a tunable phase shift between the two supply voltages. Moreover, by switching on and off power supply, the joints of the device can be locked to simulate passive stiff walls. Since USM is magnetic compatible, Flueckiger *et al.* [11] used admittance control for their haptic interface driven by the USM in magnetic resonance environment. Because the USM suffers from severe system nonlinearities and parameter variations, they proposed a speed control approach by amplitude modulation of the supply voltage to linearize the frequency-speed characteristic for the USM. To adapt to impedance control and meet the requirements of safe and smooth interaction for haptic interfaces, Chapuis *et al.* [12], [13] presented a novel MR-compatible actuator, which consists of an USM that is controlled in speed and combined with an electrorheological fluid brake. This combination can modulate the output torque over a differential gear. Sergi *et al.* [14] presented the design of a robot that can simultaneously measure, assist, and perturb movements of wrist movements during fMRI using USM. Olsson *et al.* [15] compared the walking and travelling-wave piezoelectric motors as actuators in two kinesthetic haptic grippers by virtual stiffness, virtual damper, free motion and virtual wall serials experiments. They concluded that the walking quasi-static motor is superior at low velocities and the travelling-wave ultrasonic motor is more suitable for the high-velocity applications.

In this article, we adopt the USM to further increase the stiffness of a co-actuation module. In Section II we describe the mechanical design and control for the module driven by an

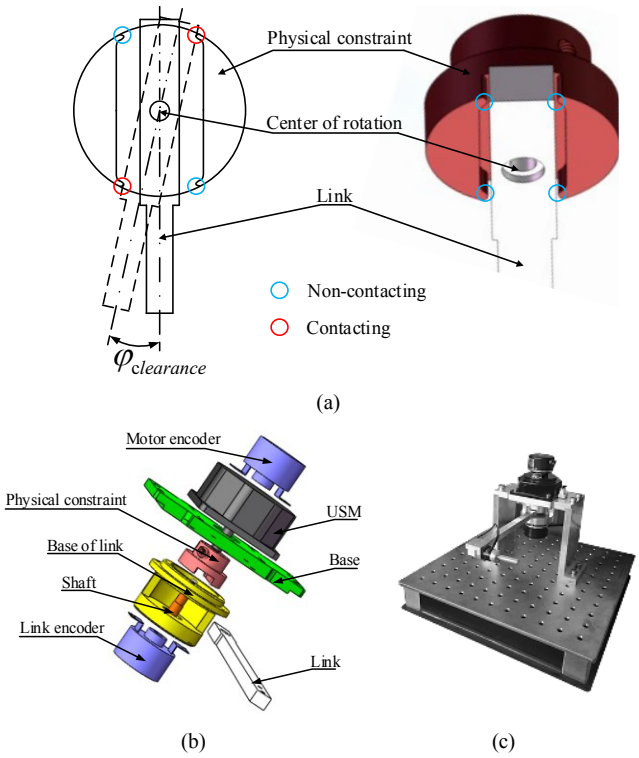

Fig. 1. The co-actuation module driven by USM. (a) The plane view of the physical constraint and the link. (b) The mechanical structure of the co-actuation module. (c) The prototype.

USM. In Section III we obtain the transfer function of the USM and its driver by system identification method. In Section IV we derive the model for clearance using the transfer function. In Section V we conduct free space and virtual wall experiments to validate the clearance model and measure the back-driving force and the maximum stiffness value. Finally, we make conclusions and discuss the future work in Section VI.

II. Co-actuation with Ultrasonic Motor

Fig. 1.a shows the working principle of a co-actuation module of one DOF. The key component in the module is the physical constraint. When the link is rotated by a user, the motor drives the physical constraint to follow the motion of the link. When simulating free motion in virtual space, the physical constraint keeps a small angle to the link. Thus, the user feels no resistance. When simulating contact between virtual objects, the physical constraint makes a contact with the link, allowing the user feel a hard contact and resistance. By co-actuation, we mean that the physical constraint is controlled to move coordinately with the link.

Since the link and the physical constraint are separated, the friction and inertia in the motor is not transmitted to the link. This results in a great reduction in inertia. Fig. 2.a shows the co-actuation module developed in [7]. We used a DC motor and a harmonic drive to generate a high force. Table I lists the inertia of each critical component in the device prototype, where J_{link} , J_{motor} , J_{gear} are the inertia of the link, the DC motor and the gear reducer, respectively. In the case of co-actuation, the inertia reflected to the user hand is $J_1 = J_{link}$. Without using co-actuation, the inertia reflected to the user hand is given by $J_2 = J_{link} + J_{gear} + J_{motor} R^2$, where R is the transmission ratio. Taking the data in Table I as example, $J_1 / J_2 = 16.8\%$, which shows the co-actuation module greatly reduces the inertia.

Fig. 2.b shows the stiffness performance of the previous prototype [7]. The first phase of the curve shows a low stiffness (10N/mm) caused by the backlash. Once the backlash is eliminated, the servo-controller starts to work and generates electrical impedances. As result, the stiffness of the second phase is high (40N/mm). To prevent the backlash from reducing the stiffness, here we use the USM as the actuator for co-actuation and investigate its effectiveness.

A. The Mechanical Structure

Fig. 1.b shows the mechanical structure of the co-actuation module. The home position of the link is defined as the center line of the physical constraint. The limiting position of the link is defined as where the link contacts the physical constraint. The clearance value $\varphi_{clearance}$ is defined as the angle between the home position and the current position of the link. The maximum clearance is the angle between the home position and limiting positon as shown in Fig. 1.a. In free space, the clearance value should always be less than the maximum clearance to avoid collision. In constraint space, which side of the physical constraint contacts the link depends on the task simulated in the virtual environment.

Fig. 1.c is the image of the prototype using the co-actuation module. The module is driven by a USM and a force sensor [16] is mounted on the end of the link. Table II gives the technical specifications of the USM, the encoders and the force sensor used in the prototype. The force sensor can measure a 3-dimensional force. We use its z-axis component to measure the normal force in the virtual wall test.

B. The Control

The control of co-actuation can be in two modes: motion tracking and constraint position control [6], [7]. In free space,

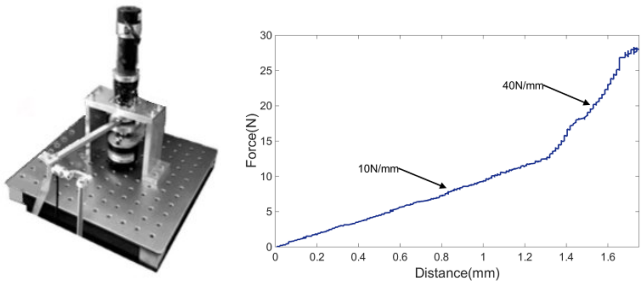

Fig. 2. Co-actuation driven by the combination of the electromagnetic motor and the gearbox. (a) The prototype. (b) The performance of stiffness when simulating a virtual wall (the rotation radius r=0.16m).

TABLE I. Co-actuation Model Using DC Motor

Component	Specification	Inertia
Motor	MAXON RE30 268214 Rated torque: 85.6mNm	3.35 kg·mm^2
Gear reducer	Harmonic drive, Ratio 50	1.20 kg·mm^2
Link	Length: 160mm	1693.63 kg·mm^2

TABLE II. CO-ACTUATION MODULE USING USM

Motor and Encoder	
Type	GTUSM-60
Rated power	6.0W
Rated torque	0.5Nm
Rated rotational speed	120rpm
Response time	<1ms
Resolution of encoder	0.022°
Force Sensor	
Type	SRI M3701
Max F_z force	100N
Non-linearity	0.5% full scale

the physical constraint is controlled to track the motion of the link and keep a desired clearance with the link. In constraint space, the controller sends a position command according to the measured force by the user (i.e. admittance control). In the two modes, the actuator is always under the position control.

The USM used is GTUSM-60 [17] (Jiangsu Glittering Orient Ultrasonic Motor Co., Ltd, China), with a position driver working at a driving frequency of 41.5KHz . The driver sends the position command via a serial port and the frequency of the servo loop is 100Hz.

III. TRANSFER FUNCTION OF THE ACTUATION SYSTEM

Determining the value of the clearance between the link and the physical constraint is a key to realize the co-actuation. On one hand, a large clearance may result in a large penetration between two objects in the virtual environment. On the other hand, a small clearance may easily lead to undesired contact in the free space. Thus, there is a trade-off in the clearance requirement between the free space and the constraint space.

In the case of electromagnetic motor, we showed that the clearance is proportional to the speed of the link [7]. Since the working principles between the DC motor and the USM is completely different, the previously obtained clearance model can no longer be applied for the USM. We need to develop a new clearance model. For this purpose, we first obtain the transfer function for the USM and its driver.

The USM contains piezoelectric conversion and friction conversion, both of which are highly nonlinear. Thus, it is difficult to develop a theoretical model for the actuator system [8], [14]. Alternatively, we use a system identification method to model the actuator transfer function.

In system identification, it is required that the input signals adequately excite the dynamics of the system. For the USM driver, In [14], the frequency domain signal was used as the input signal. In our case, generating a time domain signal is easier. Therefore, we choose a step signal and a maximal length sequence (MLS, [18]) as the input signals. In the following, we describe the experiments for identifying the transfer function of the USM and its driver.

A. Step Response

Fig. 3 shows the step response of the USM. The 7ms delay in the first step is due to the performance of the driver. The USM response is within 1ms, and arrives at the target angles at 18ms approximately. The steady state error of the system varies with the amplitude of the input step.

B. Input of Maximal Length Sequence

To identify the system transfer function, we use maximal length sequence (MLS) as the input. To generate a proper MLS for the system, we choose the following three parameters [18]:

1) The Amplitude: The amplitude of the MLS should be big enough as compared to the noise, but not too big to cause saturation. Here we empirically choose the amplitude of $\pm 2.2^\circ$ (± 100 pulses).

2) The Shift Pulse Period: To make the MLS's effective band cover the system dynamics, the shift pulse period Δ should satisfy:

$$\frac{1}{3\Delta} > f_{\max} \tag{1}$$

in which $f_{\max}$ is the cut-off frequency of the system. For the USM, the cut-off frequency is several tens to hundreds Hz [8], [12]. As the maximum command frequency of the driver is 100Hz and the driver has 7ms delay, we choose the shift pulse frequency of 50Hz, i.e. Δ is chosen to 20ms.

3) The Number of Cycles: To make the system response fall off to zero under the input of MLS, the number of cycles N should satisfy:

$$\begin{cases} N\Delta > t_s \\ N = 2^n - 1 (n = 1, 2, 3\cdots) \end{cases} \tag{2}$$

where the t_s is the time for achieving the target angle. As shown in the step response t_s is 18ms. We choose N = 15 empirically. The final MLS is shown in the lower part of Fig. 4.

C. System Identification

We fed the MLS into the system and measured the output angle as shown in the upper part of Fig. 4. We used the first half of the input and output data for estimation and the second half for validation. Using the MATLAB system identification toolbox [19], we obtained the system transfer function $T(s)$ with linear approximation of 81.94% fitness accuracy:

$$T(s) = \frac{e^{-0.007s}(179.2s + 41386)}{s^2 + 240.4s + 43170} \tag{3}$$

This transfer function is an approximate expression in low

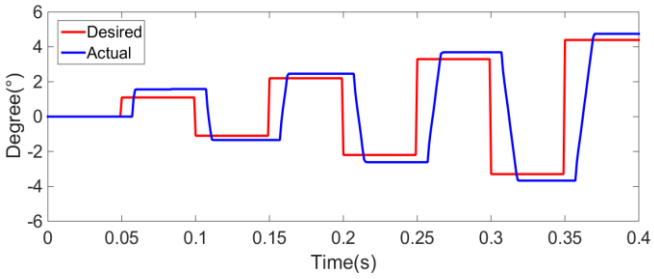

Fig. 3. The response of step input with growing amplitude. The effect of steady state error can be observed.

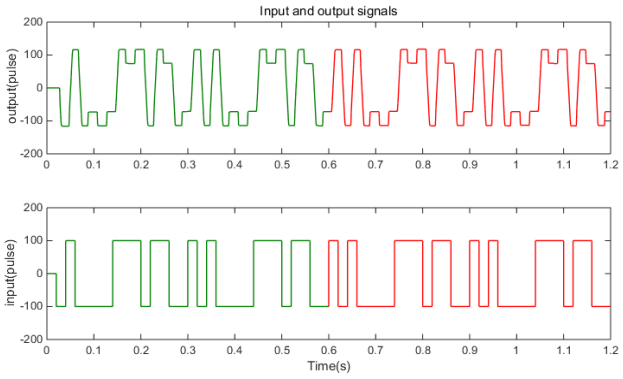

Fig. 4. The input and output signals of the system identification. (The lower part is the input of MLS. The upper part is the measured output angle. Both input and output are divided into two parts: the green is for the use of estimation and the red is for the validation.)

order of one zero and two poles with a delay portion that has the delay time of 7ms in the step response. The Bode plot of the transfer function is shown in Fig. 5, which indicates that the cut-off frequency is approximately 50Hz.

IV. The Clearance Model

As shown in the step response, the steady state error in the position control of USM is not zero. If the input speed is constant, the error between the input and the output will increase with the time. To limit the error, the input speed should change with the time. Assume the input position $r(t)$ is the sine wave:

$$r(t) = A\sin(\omega t) \tag{4}$$

Then the error between the input and the output becomes:

$$error(t) = L^{-1}[\frac{A\omega}{s^2+\omega^2}(1-T(s))] \tag{5}$$

where the L^{-1} is the inverse Laplace transform. We can derive the maximum clearance $\varphi_{maximum\_clearance}$ by:

$$\varphi_{maximum\_clearance} = \max_{t>0}(error(t)) \tag{6}$$

To find the max value, we can solve this equation:

$$\frac{derror(t)}{dt} = 0 \tag{7}$$

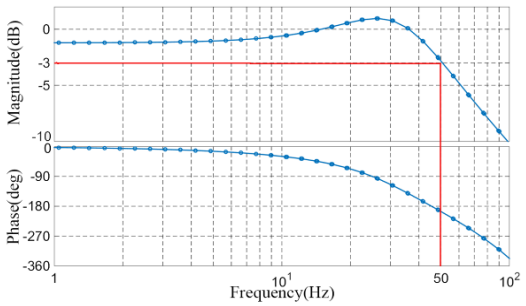

Fig. 5. The bode diagram of the transfer function obtained by system identification. The red line indicates that the cut off frequency of the system is approximately 50Hz.

In [5], it is mentioned that the bandwidth is in the range of 0~5Hz for kinesthetic interaction. For the co-actuation module shown in Fig. 1.c, the rotation range of the link is 52°, and the maximum interaction speed is 60rpm [20], hence:

$$\begin{cases} A \in [-52°, +52°] \\ \omega \in [0, \frac{2\pi}{5}] \end{cases} \tag{8}$$

Combining Eq. (3) to (8) results in:

$$\varphi_{maximum\_clearance} \approx 0.0416A \tag{9}$$

This indicates that the maximum clearance is proportional to the amplitude of the input position. It is noted that this result is obtained under the condition that the kinesthetic interaction is in low frequency range. The result can be used to guide the design and control of the physical constraint.

V. Model Validation and Performance Experiments

This section presents the experiments we conducted to validate the clearance model and evaluate the force feedback performance of the co-actuation module driven by the USM.

A. Validation of Clearance Model

For convenience, we used the part of physical constraint designed in [7], of which the maximum clearance is 1.62°. In the experiment, the operator rotates the link back and forth with increasing amplitudes until it collides with the physical limitation. During this motion, we measure the angles of the link and the physical constraint using the encoders. Fig. 6 shows that the clearance changes with the amplitudes of the link motion and the physical constraint collides with the link when the clearance becomes zero. We plot the clearance value as a function of the peak value of the operator's motion in Fig. 6.c with the following fitness line (R^2=0.9799) :

$$\varphi_{clearance} \approx 0.0464A - 0.0379 \tag{10}$$

Comparing Eq. (9) and (10), the error of proportional coefficient is found 10.3% .

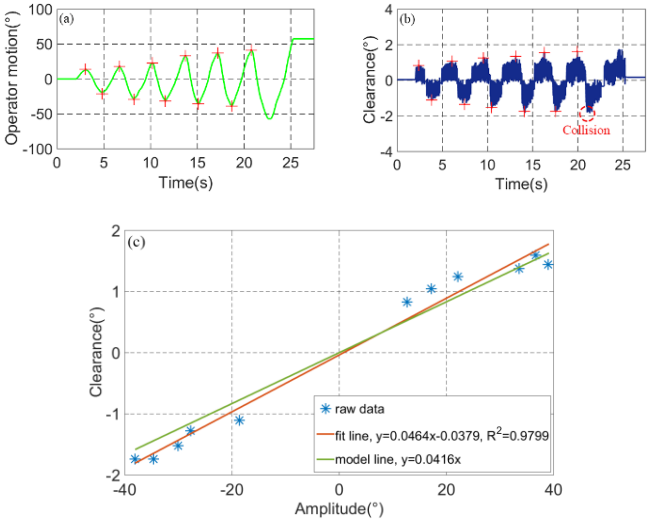

Fig. 6. The data of free space experiment to validate the clearance model. (a) The link motion (b) The varying clearance value. (c) The relationship between the amplitude and the clearance value.

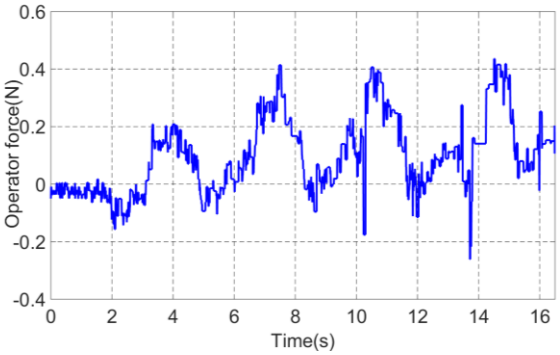

Fig. 7. The back-driving force of the co-actuation module. The maximum value is approximately 0.4N.

B. Free Motion Performance

To validate the performance of simulating free space, the operator rotates the link randomly under the condition of Eq. (8). As shown in Fig. 7, the back-driving force measured is less than 0.4N. Because the link speed is low and the rotational axis is vertical, inertia force can be ignored and the gravitation has no effect on the back-driving force. Thus, the 0.4N back-driving force is mainly due to the friction present in the joint.

C. Constrained Motion Performance

To validate the performance of simulating constraint space, we conducted a classical virtual wall experiment. A force sensor is mounted on the end of link that is 0.16m away from the rotation axis. The user moves the link to collide with the physical constraint at a pre-defined position that simulates a virtual wall. Fig. 8 shows that when the link contacts the physical constraint, the penetration distance is zero until the applied force increases to 4N, which corresponds to 4*0.16=0.64Nm. This torque is bigger than the maximum torque of the USM (0.5Nm). In this case, the USM loses the control.

As the resolution of the link encoder is 0.022 ° (i.e. 0.065mm), the stiffness $K_{stiffness}$ can be estimated by

$$K_{stiffness} = \frac{Force}{Distance} = \frac{4}{0.065} = 61.5N/mm \qquad (11)$$

The virtual stiffness simulated by the co-actuation module is

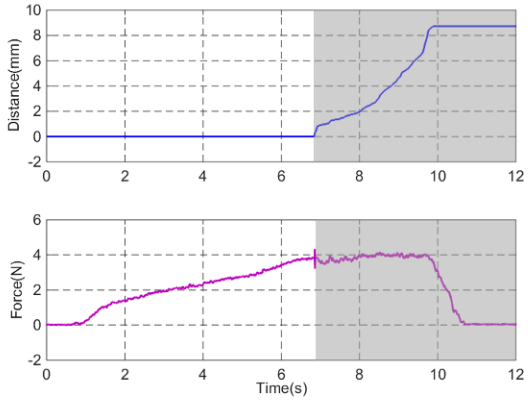

Fig. 8. The virtual wall experiment. The upper part of the figure is the penetration depth, and the bottom is the applied force. The grey area represents the zone inside the wall.

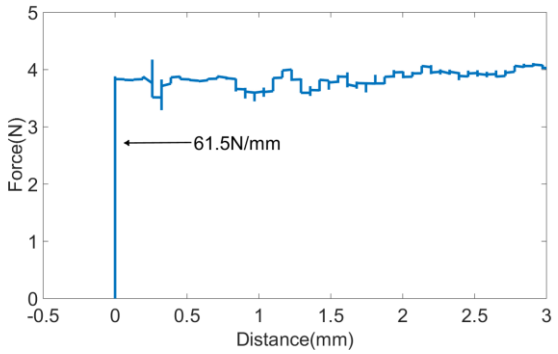

Fig. 9. The virtual wall stiffness simulated by the co-actuation module.

shown in Fig. 9. Comparing Fig. 2.b and Fig. 9, it is clear that using the USM can eliminate the effect of backlash in transmission and thus improve the stiffness performance of the co-actuation module. It is noted that the maximal torque of the current co-actuation module (0.5 Nm) is smaller than that of the previous module. To achieve the same value of the output torque, a transmission ratio of 6 is necessary.

VI. Conclusion

In principle, co-actuation method is an effective way to increase stiffness and reduce inertia of haptic devices. When using electromagnetic motor and gearbox in the co-actuation module, the backlash in the transmission leads to low stiffness in the initial contact. In this paper, we have shown that it is possible to solve this problem by using USM. Our preliminary experimental study demonstrated that the co-actuation module driven by USM has the maximum stiffness of 61.5N/mm while the back-driving friction is less than 0.4N. These results suggest that the co-actuation module driven by USM has a potential to provide both high stiffness and low back-driving force.

The key factor in the implementation of the co-actuation concept is to design a proper clearance of the physical constraint. We developed a model for the clearance under the condition of low frequency kinesthetic interaction. The model was verified through experiments. Both the model and the experiment results indicate that the clearance value is proportional to the amplitude of the link motion, and the motion speed does not affect the clearance within the range of 0~5Hz. The model can be used in the structural design of the co-actuation module for determining the maximum clearance.

Although the USM has some advantages over electromagnetic motors for the co-actuation concept, we have found some new issues in the experiment. First, the driver used to control USM is custom-designed, which is unable to achieve accurate position control. Because of this, it is difficult to generate a small stiffness value by admittance control. Second, the maximum output force is 4N, which is small to render hard contact with large force. To increase the force, cable driven transmission might be a good solution for preventing backlash. It should be noted that adding the cable mechanism does not increase the link inertia because, in the co-actuation module, the link and the physical constraint is separated.

The co-actuation method is promising for simulating hard unilateral constraints (e.g. contact with a virtual wall).

However, in implementing bilateral constraints, it will present some perceivable backlash and possible instabilities. Therefore, the approach is suited to the application requiring large stiffness or force in unilateral constraints.

In the future, we plan to improve the performance of the control system for USM. Moreover, multi DOF force feedback device with co-actuation driven by USM will be developed for the applications requiring both high stiffness and low back-driving force, such as dental surgery simulation.

ACKNOWLEDGMENT

This work is supported by National Key Research and Development Program of China under Grant No. 2017YFB1002803, and the National Natural Science Foundation of China under the grant No. 61572055 and 61532003.

REFERENCES

[1] T. Massie and J. Salisbury, "The PHANTOM haptic interface: A device for probing virtual objects," in *ASME Winter Annual Meeting, Symposium on Haptic Interfaces for Virtual Environment and Teleoperator Systems*, vol. DSC 55, Chicago, IL, 1994, pp. 295–302.

[2] K. Salisbury, B. Eberman, M. Levin, and W. Townsend, "The design and control of an experimental whole-arm manipulator," in *The Fifth International Symposium on Robotics Research*, 1990, pp. 233–241.

[3] R. Van der Linde, P. Lammertse, E. Frederiksen, and B. Ruiter, "The haptic master, a new high-performance haptic interface," in *Proc. Euro-Haptics*, Edinburgh, U.K., 2002.

[4] E. Faulring, J. Colgate, and M. Peshkin, "The Cobotic Hand Controller: Design, control and performance of a novel haptic display," *Int. J. Robot. Res*., vol. 25, no. 11, pp. 1099–1119, 2005.

[5] H. Tan, B. Eberman, M. Srinivasan, and B. Cheng, "Human factors for the design of force-reflecting haptic interfaces," in *ASME DSC*, vol. 55, no. 1, Chicago, IL, 1994, pp. 353–359.

[6] H. Zhang, Y. Zhang, D. Wang and L. Lu, "DentalTouch: A haptic display with high stiffness and low inertia," *2017 IEEE World Haptics Conference (WHC)*, Munich, 2017, pp. 388-393.

[7] J. Song, Y. Zhang, H. Zhang, and D. Wang, "Co-actuation: achieve high stiffness and low inertia in force feedback device," in *Proceedings of Euro-Haptics*, London, UK, 2016, pp. 229-239.

[8] C. Zhao, *Ultrasonic motors: technologies and applications*. New York: Springer-Verlag, 2011, ch. 1.

[9] F. Giraud, M. Amberg and B. Lemaire-Semail, "Control of a haptic interface actuated by ultrasonic motors," in *Proceedings of 14th International Power Electronics and Motion Control Conference EPE-PEMC 2010*, Ohrid, 2010, pp. T4-86-T4-89.

[10] F. Giraud, B. Semail and J. T. Audren, "Analysis and phase control of a piezoelectric traveling-wave ultrasonic motor for haptic stick application," in *IEEE Transactions on Industry Applications*, vol. 40, no. 6, pp. 1541-1549, Nov.-Dec. 2004.

[11] M. Flueckiger, M. Bullo, D. Chapuis, R. Gassert and Y. Perriard, "fMRI compatible haptic interface actuated with traveling wave ultrasonic motor," *Fourtieth IAS Annual Meeting. Conference Record of the 2005 Industry Applications Conference*, 2005, pp. 2075-2082 Vol. 3.

[12] D. Chapuis, R. Gassert, E. Burdet and H. Bleuler, "Hybrid Ultrasonic Motor and Electrorheological Clutch System for MR-Compatible Haptic Rendering," *2006 IEEE/RSJ International Conference on Intelligent Robots and Systems*, Beijing, 2006, pp. 1553-1557.

[13] D. Chapuis, R. Gassert, E. Burdet and H. Bleuler, "A hybrid ultrasonic motor and electrorheological fluid clutch actuator for force-feedback in MRI/fMRI," *2008 30th Annual International Conference of the IEEE Engineering in Medicine and Biology Society*, Vancouver, BC, 2008, pp. 3438-3442.

[14] F. Sergi, A. C. Erwin and M. K. O'Malley, "Interaction Control Capabilities of an MR-Compatible Compliant Actuator for Wrist Sensorimotor Protocols During fMRI," in *IEEE/ASME Transactions on Mechatronics*, vol. 20, no. 6, pp. 2678-2690, Dec. 2015.

[15] P. Olsson, F. Nysjö, I. B. Carlbom and S. Johansson, "Comparison of Walking and Traveling-Wave Piezoelectric Motors as Actuators in Kinesthetic Haptic Devices," in *IEEE Transactions on Haptics*, vol. 9, no. 3, pp. 427-431, July-Sept. 1 2016.

[16] www.srisensor.com.

[17] www.jszjdf.com.

[18] Torsten Söderström and Petre Stoica. *System identification*. New York: Prentice-Hall, 1989.

[19] L. Ljung, "System identification toolbox," *Matlab user's Guid*., vol. 1, p. 237, 2011.

[20] D. Wang, Y. Zhang, J. Hou, Y. Wang, P. Lv, Y. Chen, and H. Zhao, "iDental: A haptic-based dental simulator and its preliminary user evaluation," *IEEE Trans. Haptics*, vol. 5, no. 4, pp. 332–343, 2012.